



Article

Fast-, Light-Cured Scintillating Plastic for 3D-Printing Applications

Brian G. Frandsen ^{1,*}, Michael Febraro ^{2,*}, Thomas Ruland ³, Theodore W. Stephens ¹,
Paul A. Hausladen ², Juan J. Manfredi ^{1,*} and James E. Bevins ^{1,4}

¹ Department of Engineering Physics, Air Force Institute of Technology, Wright-Patterson AFB, Dayton, OH 45433, USA

² Physics Division, Oak Ridge National Laboratory, Oak Ridge, TN 37830, USA

³ Department of Physics and Astronomy, Louisiana State University, Baton Rouge, LA 70803, USA

⁴ Los Alamos National Laboratory, Los Alamos, NM 87545, USA

* Correspondence: brian.frandsen.2@us.af.mil (B.G.F.); febraromt@ornl.gov (M.F.); juan.manfredi@us.af.mil (J.J.M.)

Abstract: Additive manufacturing techniques enable a wide range of possibilities for novel radiation detectors spanning simple to highly complex geometries, multi-material composites, and metamaterials that are either impossible or cost prohibitive to produce using conventional methods. The present work identifies a set of promising formulations of photocurable scintillator resins capable of neutron-gamma pulse shape discrimination (PSD) to support the additive manufacturing of fast neutron detectors. The development of these resins utilizes a step-by-step, trial-and-error approach to identify different monomer and cross-linker combinations that meet the requirements for 3D printing followed by a 2-level factorial parameter study to optimize the radiation detection performance, including light yield, PSD, optical clarity, and hardness. The formulations resulted in hard, clear, PSD-capable plastic scintillators that were cured solid within 10 s using 405 nm light. The best-performing scintillator produced a light yield 83% of EJ-276 and a PSD figure of merit equaling 1.28 at 450–550 keVee.

Keywords: plastic scintillator; 3D printing; radiation detection



Citation: Frandsen, B.G.; Febraro, M.; Ruland, T.; Stephens, T.W.; Hausladen, P.A.; Manfredi, J.J.; Bevins, J.E. Fast-, Light-Cured

Scintillating Plastic for 3D-Printing Applications. *J. Nucl. Eng.* **2023**, *4*, 241–257.

<https://doi.org/10.3390/jne4010019>

Academic Editors: Dan Gabriel Cacuci, Bethany L. Goldblum and Thibault Laplace

Received: 5 January 2023

Revised: 17 February 2023

Accepted: 24 February 2023

Published: 7 March 2023



Copyright: © 2023 by the authors. Licensee MDPI, Basel, Switzerland. This article is an open access article distributed under the terms and conditions of the Creative Commons Attribution (CC BY) license (<https://creativecommons.org/licenses/by/4.0/>).

1. Introduction

Plastic scintillators are among the most common radiation detection materials used due to their low costs, ease of fabrication, fast response time, and ability to distinguish between neutron and gamma-ray interactions [1]. Plastic scintillators are useful for detector applications relating to national security, radiation therapy, and basic science [2,3]. The application of additive manufacturing techniques to plastic scintillators offers the potential for new and exciting uses. For instance, 3D printing allows for the fabrication of complex geometries and multi-material composites that are either impossible or cost prohibitive to produce using conventional methods.

Successful 3D printing of plastic scintillators requires the development of a printing process as well as suitable feedstock material that is similar in cost to a conventional scintillator and has mechanical, chemical, and optical properties suitable for the 3D-printing process. The combination of the feedstock and printing process will need to result in printed parts having mechanical, optical, and scintillation (light yield and pulse shape discrimination, or PSD) performance near or exceeding that of conventional plastic scintillators.

There is a wide range of 3D printing methods available, including filament-based methods, such as fusion deposition modeling (also called fused filament fabrication), powder-based laser sintering, and light-based resin curing [4]. Of the common 3D printing methods, light-based methods—that is, methods based on photopolymerization of a liquid

resin—such as stereolithography (SLA) and digital light processing (DLP) offer the best optical clarity [5]. A few researchers have developed formulations of scintillating resins that either have or can be used in light-based 3D printers, but the light yield of these scintillators was low (~35% of commercially available plastic scintillators) and PSD was not reported [6–8]. Other recent research reported a DLP 3D-printed scintillator with a light yield of up to 67% of BC-408 plastic scintillators. This formulation used bisphenol A ethoxylate dimethacrylate (BPA(EO)₁₅DMA) as the primary solvent, 1-methyl-naphthalene as the secondary solvent, 2,5-diphenyloxazole (PPO) as the primary dye, 1,4-bis(9-ethyl-3-carbazo-vinylene)-9,9-dihexyl-fluorene (ADS086BE) as the wavelength shifter, and diphenyl (2,4,6-trimethylbenzoyl) phosphine oxide (TPO) as the photoinitiator [9,10]. However, like the other light-based, 3D-printable formulations, PSD performance was not reported. Recent research was successful in producing a DLP 3D-printed plastic scintillator sample with a reported PSD FoM of 1.73 ± 0.02 from 300–1000 keVee using 30% PPO [11]. Another novel, light-cured, PSD plastic scintillator was recently reported in [12], but the required cure time of tens of minutes makes its use in 3D printing impractical, where cure times of tens of seconds or less are required for rapid prototyping and manufacturing.

The goal of this work was to create a mechanically hard, optically clear, 3D-printable (i.e., DLP or SLA), PSD plastic scintillator with a light yield comparable to commercially available PSD plastic scintillators, i.e., EJ-276 (8600 photons per 1 MeVee) [13]. This resulted in the development of a light-based, PSD-capable plastic scintillator formulation that cures in seconds using industry-standard 405 nm light and is suitable for the 3D printing of radiation detectors. In particular, this work reports the development of the fast-curing formulation, the material properties and radiation detection performance of the resulting light-cured scintillators, a parametrically optimized formulation, and an initial aging study.

2. Materials and Methods

2.1. Scintillator Development

The formulation of the resin was based on five basic components; a monomer, a crosslinker, a photo-initiator to induce photopolymerization, and primary and secondary fluorescent dyes to produce light from radiation excitation. Several compounds were evaluated as part of the formulation development for each component.

In developing a 3D printable scintillator resin, the monomer forms the base of the resin and is the largest component by mass. The monomer needs to have good optical clarity at the scintillation wavelength, exhibit high solubility for fluorescent dyes, and not lead to the quenching of the scintillation light. Monomers, such as vinyltoluene or styrene, which are primarily used in plastic scintillators [14,15], were found to exhibit low reactivity during photopolymerization [12,16,17]. Attempts to use these types of monomers resulted in cure times of >30 min to multiple hours, which is not acceptable for 3D-printing applications. Methacrylate and acrylate compounds exhibited much higher reactivity, on the order of 10s of seconds, which is suitable for 3D-printing applications. Attempts to find an off-the-shelf aromatic methacrylate or acrylate were unsuccessful. Compounds such as ethylene glycol phenyl ether acrylate, phenyl acrylate, or benzyl methacrylate resulted in either poor hardness, making mechanical polishing difficult, or poor light yield, as was the case for benzyl methacrylate which was <1000 photons per MeVee [18]. In lieu of a suitable aromatic methacrylate, or acrylate monomer, the compound isobornyl acrylate (IBOA) was chosen due to its optical clarity, low cost, high boiling point, and high glass transition temperature. For this work, $\geq 85\%$ technical-grade IBOA from Sigma Aldrich with 200 ppm monomethyl ether hydroquinone inhibitor was used.

Crosslinkers are needed to increase hardness and decrease the gel time of the photo-cured resins. Multiple crosslinkers were tested during this work, such as difunctionized 1,6-hexanediol dimethacrylate (HDDMA), bisphenol-A dimethacrylate (BPADMA), divinylbenzene (DVB), and tetrafunctionized crosslinkers, such as pentaerythritol tetraacrylate (PETA). The HDDMA was $\geq 90\%$ pure and contained 100 ppm hydroquinone as an inhibitor, BPADMA was >98% pure with no inhibitor, PETA contained 350 ppm monomethyl

ether hydroquinone as the inhibitor, and DVB was 80% pure. The photo-initiator used to start the polymerization from incident 405 nm light was TPO from Sigma Aldrich, which was 97% pure. All compounds were used as received.

For the production of light yield in the plastic scintillators, the solvents and fluors tested were EJ-309, diisopropyl naphthalene (DIN) from Eljen Technology (Sweetwater, TX, USA) (base EJ-309 solvent with no fluors), and PPO from Sigma Aldrich, which was of scintillation grade and 99% pure. 1,4-Bis(2-methylstyryl)benzene (Bis-MSB) from Sigma Aldrich (St. Louis, MO, USA), diphenyl stilbene (DPS) from Luxottica Exciton (Lockbourne, OH, USA), and Exalite 416 from Luxottica Exciton were evaluated as wavelength shifters.

The compounds for the desired formulation to be tested were weighed and placed into a 28 × 57 mm (20 mL) reaction vial. The compounds were thoroughly mixed together using an alternating combination of an ultrasonic bath and hot plate to gently warm the mixture. To reduce oxygen-induced quenching, the reaction vial was transferred to a glove box pressurized with a nitrogen atmosphere (<0.1 ppm O₂ and <1 ppm H₂O). Dissolved oxygen was removed by sparging with nitrogen for 10 min, and the reaction vial was sealed before removal from the glove box. During this process, care was taken to minimize exposure to ambient light, as the resin polymerizes with light. Next, the resin solution was cured using a commercially available 405 nm Formlabs (Somerville, MA, USA) Form Cure (estimated to be about 25 mW/cm²) and Dymax (Torrington, CT, USA) BlueWave AX-550 VisiCure (800 mW/cm²). Finally, all solid scintillators were sanded and polished using 180 grit, 400 grit, 1000 grit, and 2000 grit sandpaper and a 300 nm EXTEC alumina slurry. The dimensions of the solid scintillators were ~2.5 cm diameter and ~1.6 cm thick.

Each formulation was given a name in the format "AFITXXX" in order to track the various formulations, and all are listed in Appendix A.

2.2. Scintillator Characterization

For each scintillator, the hardness of the plastic scintillators was measured using a Shore A durometer. For the curing studies, the light emission spectrum of the scintillators was measured by a Horiba (Kyoto, Japan) FluoroMax Plus with an excitation wavelength of 380 nm.

The relative light yield and PSD figure of merit (FoM) were measured for each scintillator. For the scintillators that leached (see Section 3.2.2 for details), the hazy film was cleaned off using mild soap and water before the measurements. Each scintillator was wrapped with two layers of MIL-T-27730A PTFE tape and coupled to a 2" Hamamatsu (Shizuoka, Japan) R7724 PMT biased at -1050 V. The signals were recorded using CAEN (Viareggio, Italy) CoMPASS (version 1.5.3) software on a CAEN DT5730, a 500 MS/s, 14-bit waveform digitizer. Figure 1 plots examples of neutron and gamma waveforms from the AFIT101 plastic scintillator formulation as recorded by the digitizer. The pulse shape is similar to that of other organic scintillators. For each waveform, the pretrigger was set to 48 samples (96 ns), and the baseline was calculated using the first 40 samples (80 ns). The long gate was set to 400 ns, and the short gate was varied to optimize the PSD FoM for each scintillator. The short gate averaged approximately 23 samples (46 ns). Both the long and short gates began immediately after the 40-sample baseline window.

The relative light yield of the scintillators was compared to EJ-276 [13] and measured using the Compton edges from the 0.511 MeV (0.341 MeV) and 1.275 MeV (1.062 MeV) ²²Na gamma rays and the 0.662 MeV (0.478 MeV) ¹³⁷Cs gamma ray. The EJ-276 plastic scintillator was a bare 1" diameter × 1" long right circular cylinder, dated 30 October 2020 from the manufacturer, which has known aging degradation [15,19,20]. It was removed from its nitrogen-environment shipping container on 26 April 2021 for its first use in measurements.

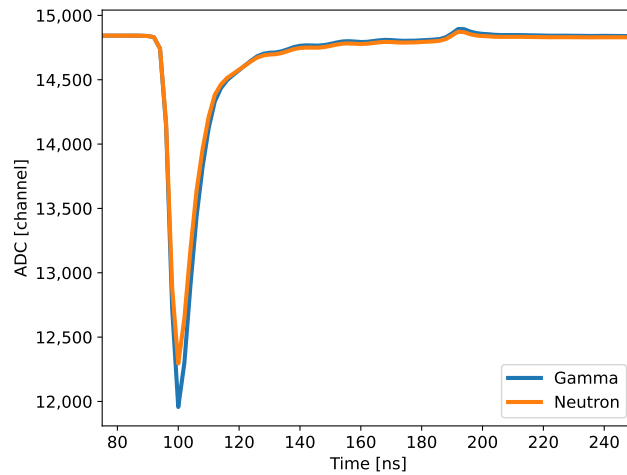


Figure 1. Example recorded waveforms for a neutron (orange) and gamma-ray (blue) event in AFIT101 using a Caen DT5730 digitizer. Each waveform is the average from all the pulses between 0.9 and 1.1 MeVee and a PSD of 0.10–0.14 for gamma rays and 0.19–0.23 for neutrons.

The Compton edge location in the recorded spectrum was determined by fitting a half-Gaussian distribution to the edge as shown in Figure 2 for the ²²Na 0.511 MeV (0.341 MeV) gamma ray in EJ-276. The Compton edge, which was used for comparing the relative light yield between scintillators, was calculated as

$$CE = \mu + \sigma\sqrt{2\ln 2}, \tag{1}$$

where μ and σ are the mean and standard deviation of the Gaussian distribution [21]. For each scintillator, including EJ-276, the average and standard deviation of each of the three Compton edges were calculated from multiple measurements of each scintillator. The relative light yield was then calculated as the ratio of the average Compton edge for each scintillator to EJ-276 for each of the three Compton edges. The reported relative light yield is an average of the three relative light yields obtained for each scintillator for the three Compton edges measured.

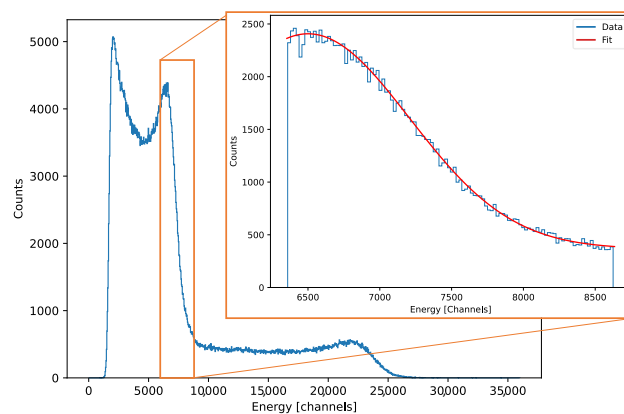


Figure 2. An example ²²Na pulse integral spectrum from EJ-276 illustrating the half-Gaussian fit to the 0.511 MeV gamma-ray Compton edge (0.341 MeV).

This approach in locating the Compton edge introduces potential bias [22] and does not take into account effects such as multiple scattering [23]. Since this potential bias was comparable in the scintillators and EJ-276 measurements (<0.5% difference), calculating relative light yield minimizes the potential impact of this bias [22].

Second, neutron and gamma-ray induced events were discriminated using the waveform charge integration PSD as shown in Figure 3a [24]. After calibrating the energy of

the spectrum using the Compton edges from the 0.511 MeV, 0.662 MeV, and 1.275 MeV gamma rays, a PSD histogram was generated from the events between 450 and 550 keVee. The histogram was then fit with two Gaussians, shown in Figure 3b, and the quality of the PSD was quantified using a FoM given as [24,25]

$$\text{FoM} = \frac{\mu_2 - \mu_1}{\text{FWHM}_2 + \text{FWHM}_1}, \quad (2)$$

where μ and FWHM are the mean and full-width at half-maximum for each of the Gaussian distributions, respectively.

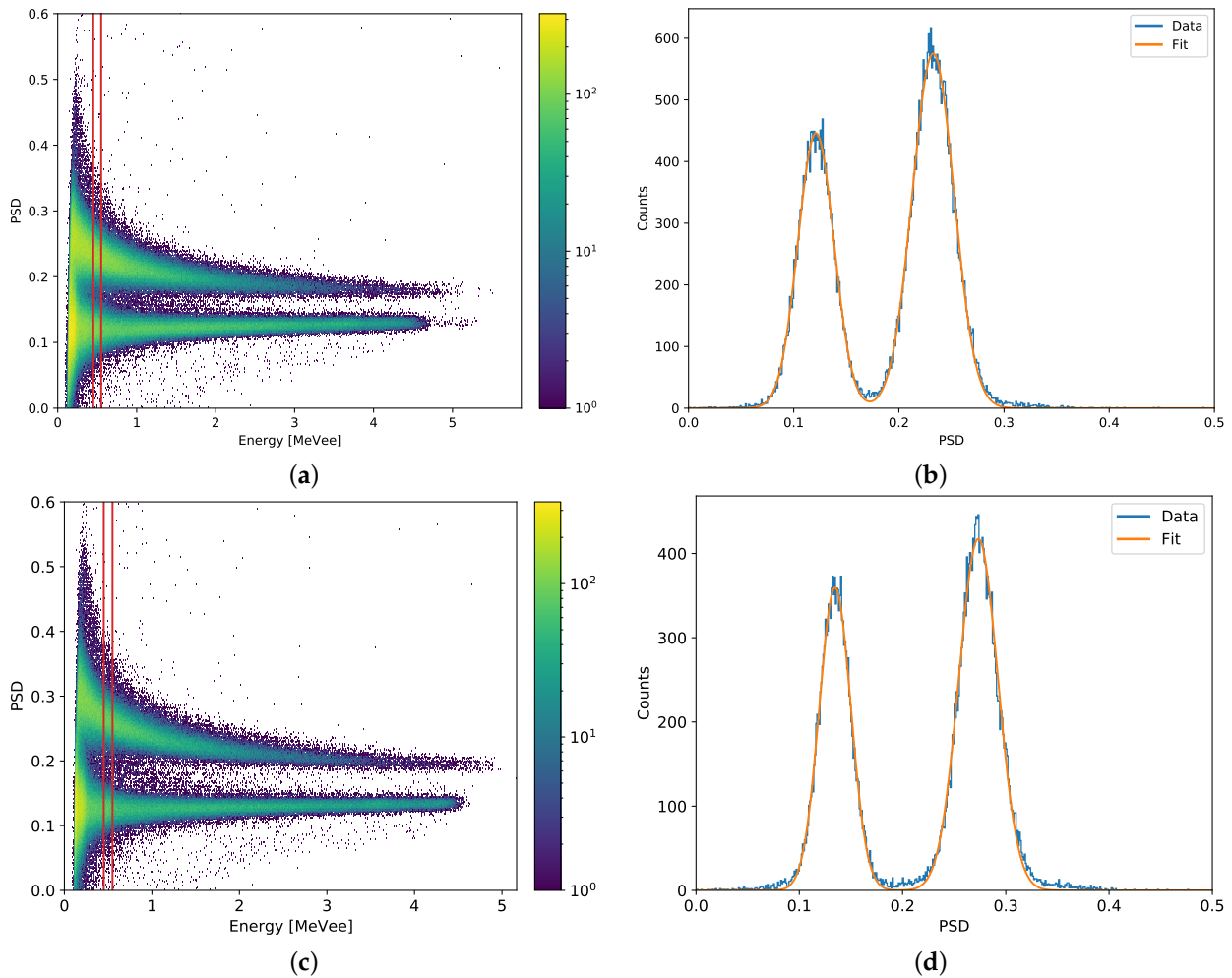


Figure 3. 2D PSD/energy histogram from exposing (a) AFIT101 and (c) EJ-276 to an AmBe source. A cut was made over the 450 and 550 keVee range, represented by the red lines, to generate a 1D AmBe PSD histogram, where a double Gaussian fit was used to calculate the PSD FoM according to Equation (2) for (b) AFIT101 and (d) EJ-276. The colorbar represents the number of counts.

2.3. Exploratory Formulation Studies

A step-by-step, trial-and-error approach was taken to identify promising combinations to achieve a formulation that would create a mechanically hard, optically clear plastic with high light yield and neutron/gamma-ray discrimination. While not an exhaustive search of the parameter space, the series of small studies led to a promising general formulation that was then parametrically optimized as described in Section 2.4. All samples were approximately 10 g (~2.5 cm diameter and ~1.6 cm thick), and the formulations, Table A1 and Table A2, are shown in Appendix A for the key steps and formulations described below.

The first study explored the compatibility of different wave shifters with the 405 nm cure light and primary solvents. Three samples (AFIT002-004) were created with 0.2 wt% of Bis-MSB, Exalite 416, and DPS, respectively. The other chemicals in the scintillators were kept constant for all three. The DPS did not dissolve into the solution. The scintillator with Bis-MSB was solid throughout but softer in the center, while the Exalite 416 formulation was consistently hard throughout. It was determined that the Bis-MSB had a higher absorption at 405 nm, shown in Figure 4, preventing the light from penetrating the entire depth of the resin and obtaining a complete cure. Therefore, Exalite 416 was selected as the wave shifter for all future formulations.

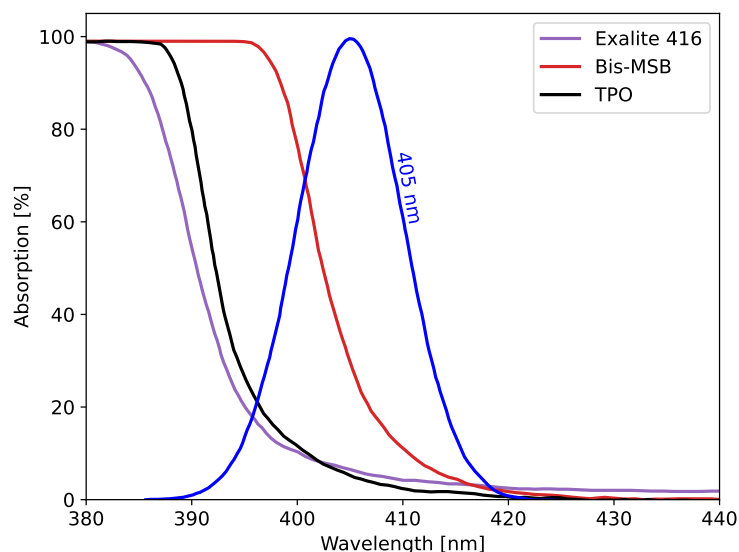


Figure 4. The light absorption of the secondary dyes, Exalite 416 (purple) and Bis-MSB (red), and of the photoinitiator, TPO (black), compared to the measured emission spectrum of the 405 nm cure light (blue). The concentration of the Exalite 416 (0.2 wt%; 0.0022 mol/L), Bis-MSB (0.2 wt%; 0.0051 mol/L), and TPO (0.1 wt%; 0.0023 mol/L) were the same concentrations used in the scintillators, and the solvent was spectroscopic-grade ethanol.

In the next step, the ratio of plastic-forming to light-yielding compounds was switched to 60/40 to increase the light yield of the scintillator. Reduced crosslinker concentration had previously been observed to result in soft, gummy-like cures, while high crosslinker concentrations led to cloudy scintillators. Therefore, the solid BPADMA was replaced with liquid HDDMA to explore formulations that lead to a harder, clearer plastic since the liquid HDDMA better dissolved and did not precipitate out of the solution. Three formulations with different IBOA/HDDMA ratios (70/30, 60/40, and 50/50) were explored. The formulations with the 60/40 and 50/50 IBOA/HDDMA ratios (AFIT013 and 014) yielded cloudy scintillators. The formulation with the 70/30 IBOA/HDDMA ratio (AFIT009) was clear but too soft, similar to hard rubber. PETA and DVB crosslinkers were also tried but did not provide better results than HDDMA or BPADMA. Additionally, all attempts to use DVB or any vinyl monomer significantly increased the required cure time.

Therefore, an IBOA/HDDMA ratio of 70/30 was used for future formulations, and variations were made to improve the hardness and radiation detection performance. First, the amount of light-yielding compounds was reduced to improve the hardness of the plastic. Two formulations (AFIT016 and 017) were developed with 30 wt% (70 wt% IBOA and HDDMA) and 20 wt% (80 wt% IBOA and HDDMA) light-yielding compounds. The Exalite 416 and TPO were held the same at 0.2 wt% and 0.1 wt%, respectively. Second, the amount of Exalite 416 was doubled from 0.2 wt% (AFIT016) to 0.4 wt% (AFIT022). Third, an approximately 50/50 ratio of HDDMA and BPADMA (AFIT023) was tested as the crosslinker. Each of these was sequentially cured for 4–5 min in a Formlabs Form Cure, followed by 1 min in the Dymax BlueWave AX-550 VisiCure, and then sanded and polished.

An increase in the plastic-forming compounds to 70–80 wt% and the addition of the BPADMA crosslinker (AFIT023) resulted in scintillators that were harder than the baseline 60/40 (plastic-forming/light-yielding compounds) ratio (e.g., AFIT013). The radiation detection performance of these scintillators demonstrated reasonable light yield (58–65% of EJ-276) and PSD (FoM between 0.74 and 1.07). It was observed that increasing the light-yielding compounds above a combined total of 30 wt% did not provide more light yield, attributable to the scintillator's reduced clarity, but it did improve the PSD performance. However, a reduction to 20 wt% of light-yielding compounds did result in a ~5% reduction in light yield and a ~16% reduction in PSD performance. Doubling the amount of Exalite 416 only slightly increased the light yield. Finally, the addition of BPADMA with HDDMA resulted in similar light yield and PSD performance. While it was observed that the scintillator with an 80/20 ratio of plastic-forming to light-yielding compounds was the clearest and hardest, it had a relatively low light yield and PSD FoM. Thus, a 70/30 ratio of plastic-forming to light-yielding compounds was carried forward.

2.4. Two-Level Factorial Parameter Study

The initial formulation development was successful in creating an optically clear and mechanically hard plastic with reasonable light yield and PSD. A two-level factorial parameter study of the fluors (DIN and PPO) and crosslinkers (HDDMA and BPADMA) was developed to analyze the effects of increasing the BPADMA crosslinker and PPO to find the locally optimal formulation to prevent leaching and allow the highest light yield output. One level inversely varied the amount of PPO and DIN, which replaced the EJ-309 from the initial formulation development, while maintaining the combined PPO and DIN contribution at 30 wt% of the mass of the scintillator. The other level inversely varied the amount of HDDMA and BPADMA from 0 to 21 wt%, maintaining the combined mass of IBOA and crosslinker at 70 wt% and the IBOA to crosslinker ratio of 70/30. The remaining chemicals were the same for each of the scintillators: IBOA was 49 wt%, Exalite 416 was 0.2 wt%, and TPO was 0.1 wt%. This resulted in thirteen scintillators—formulations shown in Table A3 of Appendix A—developed with the same procedures described in Section 2.1. These scintillators were cured for 5 min in a Formlabs Form Cure (solid in 10–20 s) followed by 4 min in the Dymax BlueWave AX-550 VisiCure to burn up the remaining TPO in the scintillators and sanded and polished.

3. Results and Discussion

3.1. Curing

The obtained light yield was dependent on the curing parameters, as residual TPO can remain after the initial curing in TPO-based light-cured materials. To understand the effects of light yield as a function of the total curing dose and ensure the curing process resulted in a scintillator with the maximum light yield, a formulation representative of the final samples was placed in a glass cuvette and cured in the Formlabs Form Cure for 5 min and Dymax BlueWave AX-550 VisiCure for 4 min (total times). At periodic intervals during the curing process, the cuvette was removed from the Form Cure or BlueWave and placed in a Horiba FluoroMax Plus to measure the emission spectrum of the scintillator while being excited at 350 and 380 nm, asynchronously. An excitation of 380 nm is sufficient for addressing the competition between TPO and secondary fluor absorption. Figure 5a plots the emission spectrum of the plastic scintillator at the different integrated curing times from the excitation wavelength of 380 nm. Figure 5b plots the intensity of the peak emission as a function of time during the curing process for 380 nm excitation light.

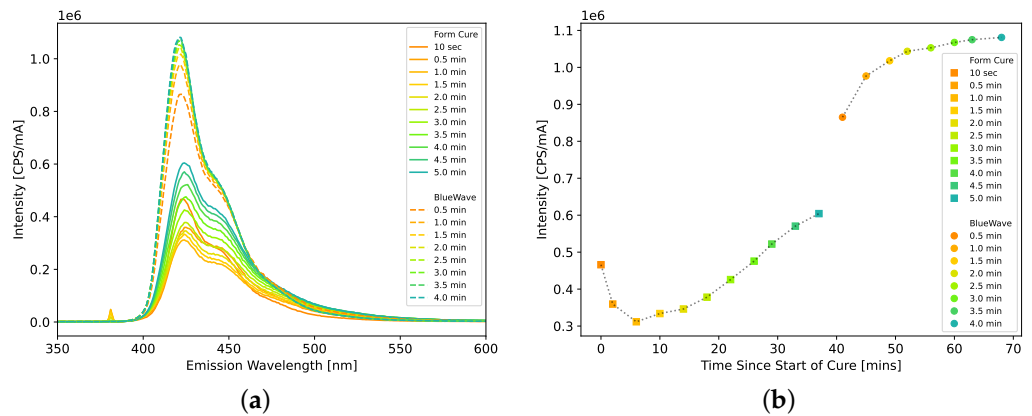


Figure 5. Photoluminescence (a) emission spectra and (b) maximum peak intensity of a representative sample excited with 380 nm light as a function of integrated curing times in the Formlabs Form Cure followed by the Dymax BlueWave AX-550 VisiCure. There was a slight shift from 425 to 421 nm in the peak emission wavelength over the duration of the curing process. Note, the time since cure in (b) includes the time to cure and measure the sample between each step.

The light emission from the scintillator first decreased during the first minute of curing in the Form Cure, then increased during the remaining duration of the curing process in the Form Cure and BlueWave. After the 4-min curing in the BlueWave, the maximum photoluminescence yield was obtained, and the peak emission increased by 55% and 79% for the 350 and 380 nm, respectively, compared to a 5-min cure in the Form Cure alone. The increase in the photoluminescence yield was attributed to increased TPO burn-up, as the samples were solid after ~10–20 s.

3.2. Observational Characterization

The observational characterization of the scintillators developed as part of the parameter study included measuring the hardness of the scintillators and visual observations of purpling, leaching, surface cracking, and reduced clarity. The hardness, surface cracking, and leaching results are shown in Figure 6, along with the two-factor formulation matrix utilized for this parameter study. There is a degree of polymerization reaction in UV curing that does not completely cure, which can cause lower hardness and degradation by oxidation (presence of unreacted double bonds). A clear trend is seen with higher PPO concentrations leading to increased leaching and reduced surface cracking.

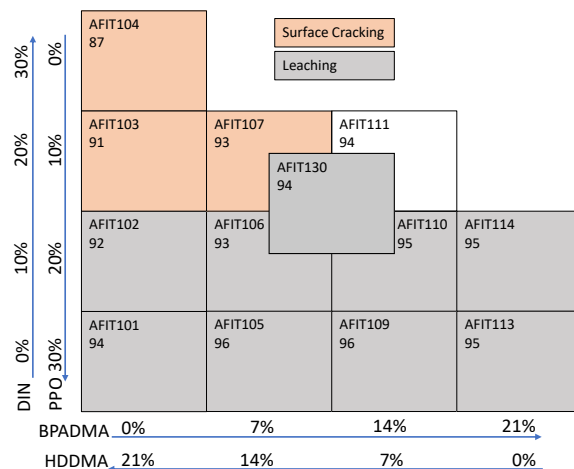


Figure 6. Shore A hardness (indicated by the value within each box), surface cracking, and leaching from the scintillators in the parameter study. A clear trend is seen with higher PPO concentrations leading to increased leaching and reduced surface cracking.

3.2.1. Purpling

It was observed that some of the scintillators became purple upon exposure to the cure light. The purple color intensity and duration increased with the amount of PPO, as shown in Figure 7 of AFIT025 and AFIT026, which contained 20 wt% and 25 wt% PPO, respectively. This purple color did dissipate with time, with the decay time varying from being on the order of minutes to a few weeks. The decay time for the purpling to dissipate increased for increasing PPO concentration and increasing BPADMA concentration, as illustrated in Figure 7, where the purple color in AFIT113 (21 wt% BPADMA) can still be seen after 3 weeks.

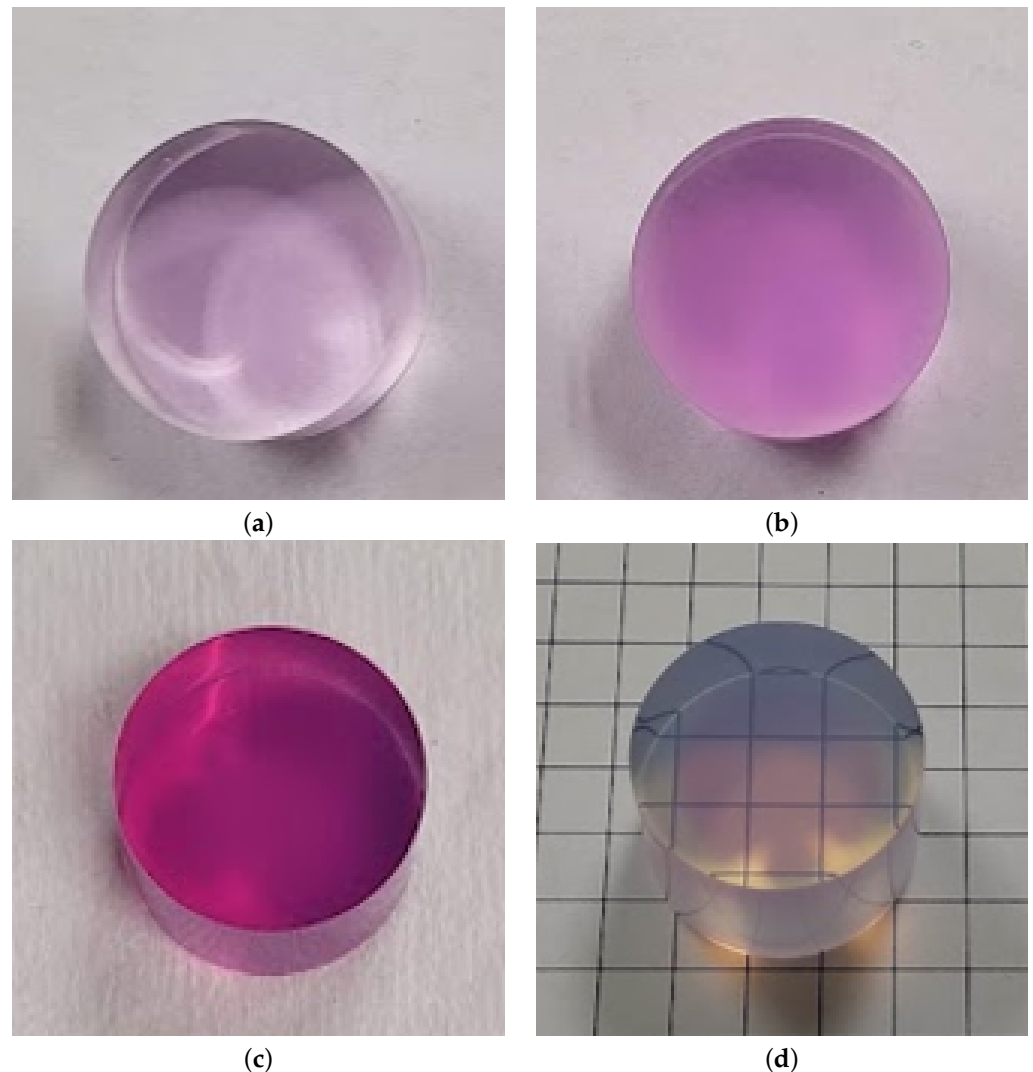


Figure 7. The intensity of the purple color observed increased with increased PPO concentration as illustrated by (a) AFIT025 (20 wt% PPO) and (b) AFIT026 (25 wt% PPO). The duration of the purpling, which varied based on the PPO and BPADMA concentration, faded away over time as illustrated in (c) AFIT113 (30 wt% PPO and 21 wt% BPADMA) shortly after being cured and (d) 3 weeks after being cured.

The direct cause of the purpling effect was not determined, but it appears to be related to an interaction between PPO and TPO. Methods to accelerate the dissipation were explored, the most promising being a heat treatment. To test this treatment, three scintillators were made with the same formulation as AFIT101. One was placed in a 4 °C refrigerator, one was left on the counter at room temperature, and another was placed in a 60 °C oven. After a couple of hours, the scintillator from the refrigerator and

room temperature maintained similar levels of purpling. However, the purple color in the scintillator from the oven had significantly faded, indicating that a post-cure heat treatment can be used to accelerate the dissipation of the purpling effect and obtain steady-state performance.

The scintillator light yield was reduced while purpling was observed in the scintillator, even for the slight purpling shown in Figure 8. When there was still purpling observed in AFIT230A (30 wt% PPO, 0 wt% DIN), Figure 8a, the relative light yield was 67%. After the purpling faded away, Figure 8b, the relative light yield increased to 71%. The difference increased as the amount of purpling present increased.

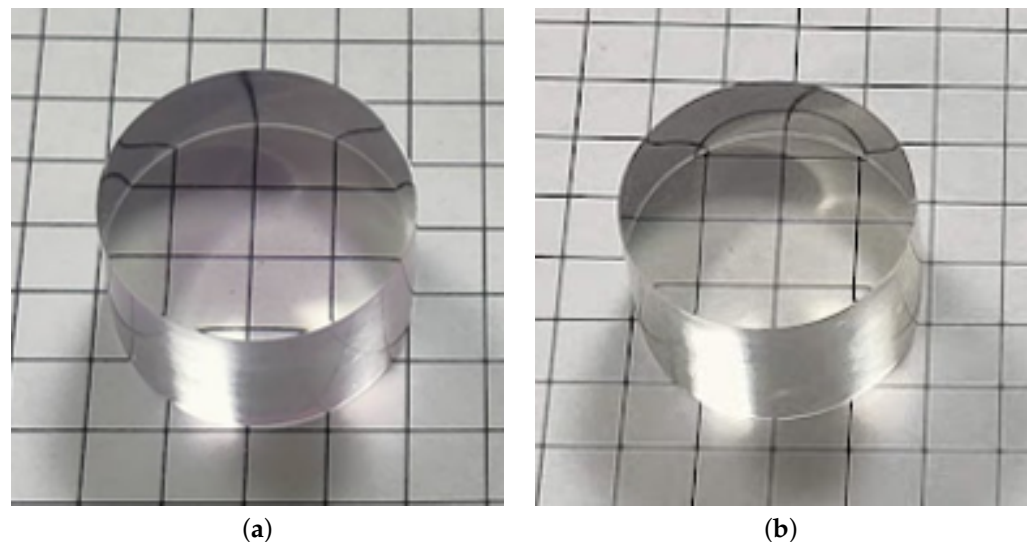


Figure 8. Purpling observed in AFIT230A (a) 6 days after being produced but not at (b) 12 days.

The light emission of AFIT131 was measured after the plastic was completely cured to better characterize the post-cure light emission. Measurements of the emission spectrum of the scintillator were taken for up to 7 h post-cure, while being excited at 350 and 380 nm, asynchronously, using a Horiba FluoroMax Plus. Figure 9a plots the emission spectrum of the plastic scintillator as a function of time after the curing process from an excitation wavelength of 380 nm. The light emission was fairly constant for the first 90 min post cure and then increased, as plotted in Figure 9b. This increase in the peak emission did not stop at 7 h post-cure. This is attributed to the dissipation of the purpling in the scintillator, and the timescales correlate well to significant observational reductions in scintillator purpling.

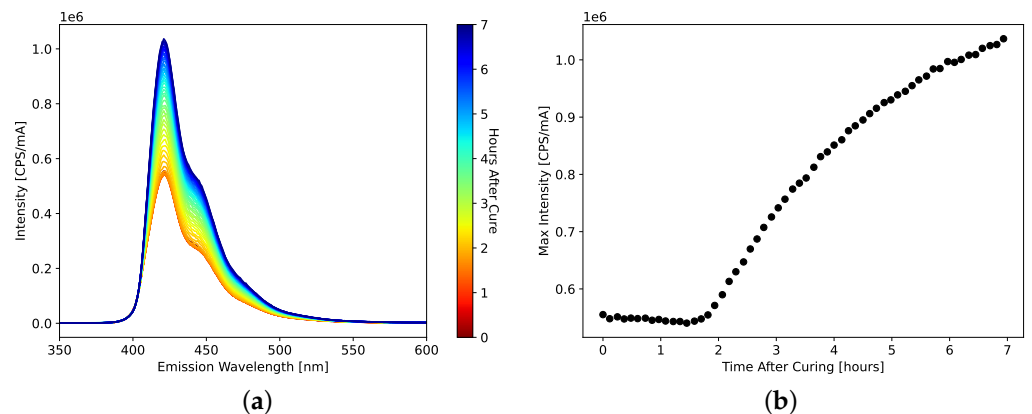


Figure 9. (a) Light emission spectra and (b) peak light emission from AFIT131 using a Horiba FluoroMax Plus with an excitation wavelength of 380 nm. There was no shift in the peak emission wavelength over the duration of the measurements.

3.2.2. Leaching

In addition to the purpling, the scintillators with higher PPO amounts (above 10 wt%) leached and created a hazy, white film on the surface of the scintillators proportional to the PPO concentration. Figure 10 shows AFIT026 (25 wt% PPO) and AFIT114 (20 wt% PPO) with the hazy film from the leaching and the clear scintillators after being washed using mild soap and water. After washing, the scintillators continued to leach and again developed the hazy film on the surface within tens of minutes to hours (≥ 20 wt% PPO) or days (15 wt% PPO). Additionally, the BPADMA, such as in AFIT114, did not prevent the leaching as compared to AFIT026, which contained HDDMA.

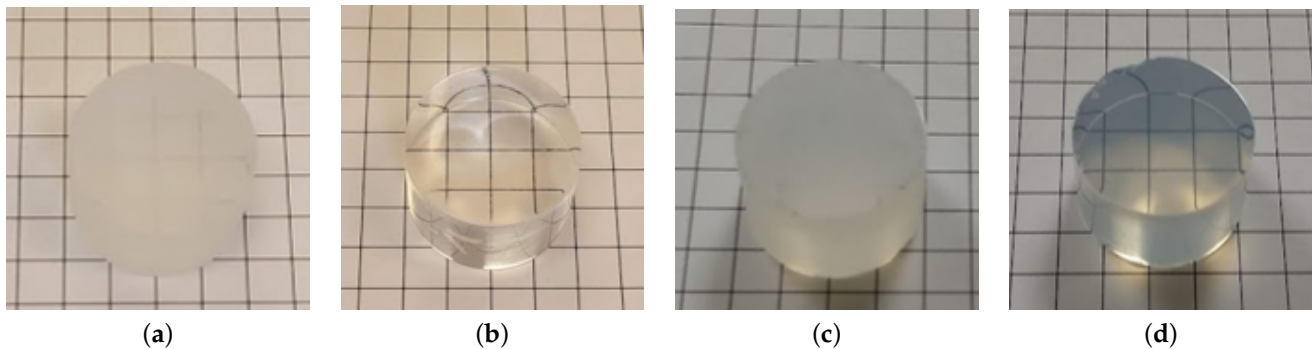


Figure 10. Hazy film from PPO leaching on (a) AFIT026 and (c) AFIT114 before and (b,d) after being washed using mild soap and water. The BPADMA in AFIT114 did not prevent the leaching as compared to AFIT026, which contained HDDMA.

3.2.3. Surface Cracking and Reduced Clarity

The softer scintillators exhibited surface cracking, as shown in Figure 11a,b of AFIT016 and AFIT104, which continued to degrade the integrity of the plastic over time. The scintillators with more than 10 wt% PPO did not crack on the surface, and the increase in BPADMA prevented surface cracking at a 10 wt% PPO concentration as observed in AFIT111. Unfortunately, the increase in BPADMA did not prevent leaching, and it did reduce the optical clarity of the scintillator, as shown in the difference between AFIT101 (0 wt% BPADMA), Figure 11c, and AFIT113 (21 wt% BPADMA), Figure 11d, after both were washed.

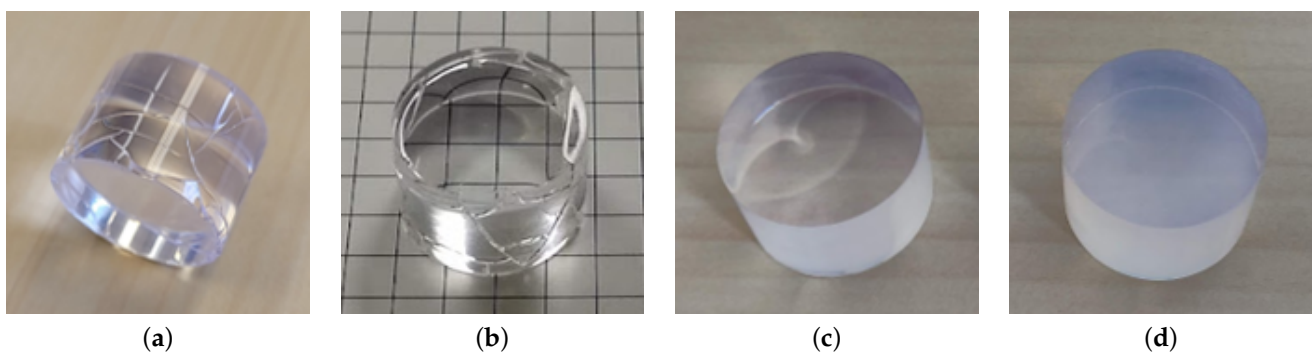


Figure 11. Surface cracking was observed in softer scintillators such as (a) AFIT016 and (b) AFIT104. While BPADMA did increase hardness and prevent cracking, it led to reduced clarity as illustrated by (c) AFIT101 (0 wt% BPADMA) compared to (d) AFIT113 (21 wt% BPADMA).

3.3. Radiation Detection Performance

Figure 12a,b show the light yield relative to EJ-276, PSD FoM, and the associated trends for several candidate formulations. The relative light yield was compared to the average of eight measurements of EJ-276 from 30 June to 1 September. These scintillators obtained a relative light yield of up to 78% of EJ-276 and a PSD FoM of 1.31 (74% of EJ-276)

in the 450–550 keVee bin. The smaller size of these scintillators, compared to the size of the EJ-276, may have caused an overestimation of the relative light output due to the lesser self-absorption of these smaller scintillators. This overestimation is no more than 10%, using an analogous comparison of BGOs of different sizes [26], and the offset (<0.5% difference) would be similar across all formulations tested as discussed in Section 2.2. A minimum FoM value of 1.27 was used as a reference parameter to define efficient neutron/gamma PSD [14]. Although organic crystals and liquids generally have better PSD performance than plastics, for the purpose of this work, we compare to the state-of-the-art plastic EJ-276. The measured EJ-276 PSD FoM was 1.78.

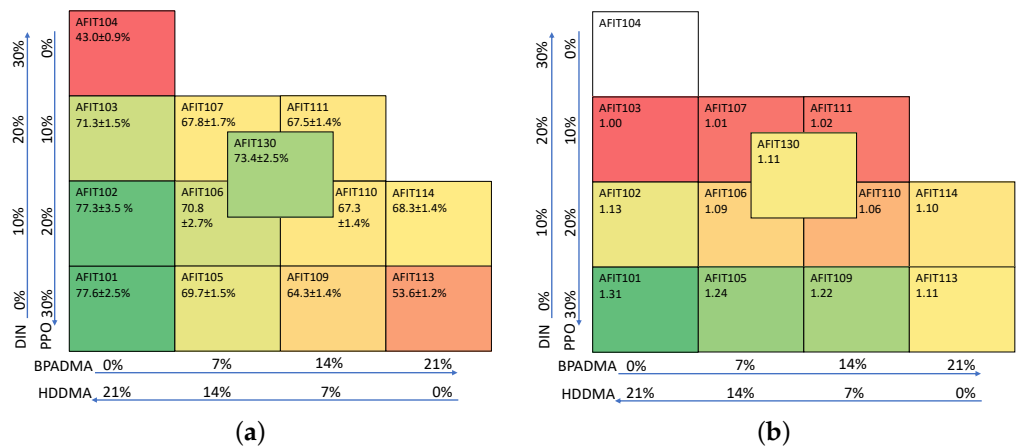


Figure 12. Radiation detection performance of the scintillators used for the parameter study. Formulation matrix of the scintillators in the parameter study with the associated (a) relative light yield compared to EJ-276 and (b) PSD FoM. The measured EJ-276 PSD FoM was 1.78.

The increase in PPO increased the light yield and PSD FoM for a set combination of crosslinkers, though it did increase the oxidation sensitivity. Unfortunately, the increase in BPADMA, while generally resulting in harder scintillators, did not prevent the leaching and reduced the clarity of the scintillators, thereby decreasing the light yield and PSD FoM. Overall, AFIT101 was found to be the best formulation for simplicity (fewer compounds used), radiation detection performance, and overall hardness and integrity over time.

3.4. Aging

AFIT101 leached quickly and significantly, raising questions about the stability of the scintillator’s performance over time. Figure 13 shows the relative light yield of AFIT101 and AFIT102 from 30 June to 15 November. Over 4.5 months, AFIT101 and AFIT102’s relative light yield decreased by 4.3% and 7.8%, respectively. The light yield in EJ-276 has also been shown to decrease over time. Compared to EJ-309, the relative light yield of EJ-276 decreased from 79% to 62% over 13 months [15,19,20], a 21.5% decrease. Over the 4.5 months observed in this study, a decrease of 5.5% was observed in the EJ-276 light yield.

The uncertainty reported in Figure 13 for AFIT101 on 12 July includes the variance from five measurements of the AFIT 101 light yield, the variance from eight measurements of EJ-276, and the associated fit methodology uncertainty. As the systematic uncertainty observed associated with the measurement and mounting each scintillator was comparable, all of the other reported uncertainties were based on the fit uncertainty for one measurement of the scintillator and the systematic uncertainty from eight measurements of EJ-276.

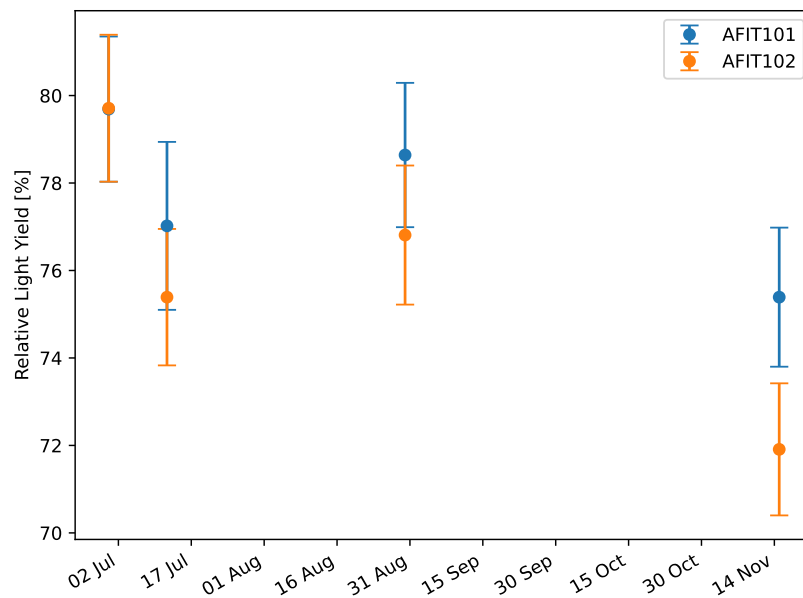


Figure 13. Relative light yield of AFIT101 and AFIT102 compared to EJ-276 from 30 August to 15 November. The error bars represent the standard deviation of the measurements.

3.5. Leaching and Ethanol Treatment

While the initial results with the formulations presented in this work do not seem to indicate a significant performance degradation over time, a potential advantage over EJ-276, the leaching of some formulations poses a challenge for printing and application use. The leaching is primarily from the PPO near the surface that crystallizes, creating the hazy film. In the Lawrence Livermore National Laboratory's development of PSD plastic scintillators, leaching was also observed on the surface of the scintillators [15]. To prevent the leaching, Zaitseva et al. developed a method to treat the scintillators with ethanol post cure. While the specifics of this treatment were not described in [15], a study was performed on the effects of an ethanol treatment on the light-cured scintillators in an attempt to reduce the leaching of PPO over time.

Four formulations were produced for the study that contained 49 wt% IBOA, 0.2 wt% Exalite 416, 0.1 wt% TPO, and 0–10% DIN, 20–30% PPO, 14–21% HDDMA, and 0–7% BPADMA as listed in Table A4. Each ~20 g formulation was prepared as described in Section 2.1 before being split equally into two separate glass containers inside the glove box. Each scintillator was cured for 5 min in the Formlabs Form Cure and 4 min in the Dymax BlueWave AX-550 VisiCure, sanded and polished. One of the scintillators from each pair was placed in a 200-proof ethanol bath for 1 h, and the other was left at room temperature in a standard atmosphere. Each treated sample showed no evidence of leaching, while the untreated sample leached as expected. The untreated sample was washed with mild soap and water (as described previously), and both samples were characterized.

The scintillators were weighed before and after the ethanol treatment to measure the amount of material that was removed by treatment before mounting them to PMTs as described in Section 2.2. The ethanol treatment resulted in relative light yield and PSD performance statistically consistent with the untreated scintillators as shown in Table 1.

Table 1. Radiation detection performance of ethanol-treated and untreated scintillators.

Scintillator	Rel. Light Yield [%]		PSD FoM	
	Treated	Untreated	Treated	Untreated
AFIT230	74.8 ± 1.8	72.3 ± 1.6	1.26	1.25
AFIT225	83.0 ± 2.1	82.2 ± 2.3	1.28	1.28
AFIT220	77.5 ± 1.8	77.8 ± 2.3	1.13	1.15
AFIT221	75.7 ± 1.7	74.3 ± 1.7	1.14	1.12

The ethanol treatment did not remove a significant amount of material (0.2–0.37% by mass); this is an expected result, as the overall composition is similar and the removed material likely was poorly incorporated into the matrix. Importantly, no visual observation of subsequent leaching has been observed in any ethanol-treated scintillator to date (>5 months), while the non-treated samples continue to leach.

4. Conclusions

This research developed fast-, light-cured plastic scintillator formulations that can be used for light-based 3D printing using industry-standard 405 nm light. The most promising formulations for creating a clear and hard plastic contained a combined total of EJ-309/DIN and PPO of 30 wt% and a combined total of IBOA and crosslinker of 70 wt% with a IBOA/crosslinker ratio of 70/30. The plastic scintillators were generally solidified within 10–20 s in the 405 nm light from a Formlabs Form Cure. The scintillator with 25–30 wt% of PPO provided the highest radiation detection performance with the light yield up to 83% of that of EJ-276 and up to a PSD FoM of 1.31. We interpret this result to show that it is possible to produce a fast, 405 nm light-cured formulation through this novel approach that compares favorably with EJ-276. The leaching and a hazy film that developed on these high PPO scintillator formulations were eliminated by placing the scintillators in an ethanol bath for 1 h. The overall best-performing scintillator was AFIT225B, which contained 5 wt% DIN, 25 wt% PPO, 21 wt% HDDMA, 0.2 wt% Exalite 416, and 0.1 wt% TPO, did not leach due to the ethanol treatment, and produced a relative light yield of 83% of EJ-276 and PSD FoM of 1.28. Other noted issues, such as surface cracking, haziness, and purpling, were addressed through improved formulations and post-cure heat treatments.

Future work includes further analysis of the effects of light yield due to curing time and TPO burn-up, a continuation of the formulation development to prevent leaching and/or increase radiation detection performance, and the production of a scintillator using a light-based 3D printer.

Author Contributions: Conceptualization, B.G.F., M.F., P.A.H. and J.E.B.; methodology, B.G.F., M.F., J.J.M. and J.E.B.; software, B.G.F.; validation, B.G.F. and T.W.S.; formal analysis, B.G.F. and T.W.S.; investigation, B.G.F., T.R. and T.W.S.; resources, M.F., P.A.H. and J.E.B.; data curation, B.G.F.; writing—original draft preparation, B.G.F. and J.E.B.; writing—review and editing, M.F. and J.J.M.; visualization, B.G.F.; supervision, J.E.B., M.F. and J.J.M.; project administration, J.E.B. and M.F.; funding acquisition, M.F., P.A.H. and J.E.B. All authors have read and agreed to the published version of the manuscript.

Funding: This research was supported by the Defense Threat Reduction Agency under grant HD-TRA1136911, U.S. Department of Energy, Office of Science, Office of High Energy Physics, under Award Number DE-AC05-00OR22725, and the ORNL Laboratory Directed Research Development Program.

Institutional Review Board Statement: Not applicable.

Informed Consent Statement: Not applicable.

Data Availability Statement: The radiation performance data from the two level-factorial parameter study (AFIT101-130) and ethanol treatment study (AFIT220-230) of this research are publicly available at <https://doi.org/10.5281/zenodo.7489982>.

Conflicts of Interest: The authors declare no conflict of interest.

Abbreviations

The following abbreviations are used in this manuscript:

Bis-MSB	1,4-bis(2-methylstyryl)benzene
BPADMA	bisphenol A dimethacrylate
DIN	diisopropyl naphthalene
DLP	digital light processing
DPS	diphenyl stilbene
DVB	divinylbenzene (DVB)
FoM	figure of merit
HDDMA	difunctionized 1,6-hexanediol dimethacrylate
IBOA	isobornyl acrylate
PETA	pentaerythritol tetraacrylate
PPO	2,5-diphenyloxazole
PSD	pulse shape discrimination
SLA	stereolithography
TPO	diphenyl (2,4,6-trimethylbenzoyl) phosphine oxide

Appendix A. Scintillator Formulations

Table A1. BPADMA-based scintillator formulations used for the first round of exploratory formulation studies to select the wavelength shifter.

Scintillator	Component Fraction in Scintillator [wt%]						
	PPO	Bis-MSB	Exalite	DPS	IBOA	BPADMA	TPO
AFIT002	15	0.2	-	-	59.5	25.5	0.1
AFIT003	15	-	0.2	-	59.5	25.5	0.1
AFIT004	15	-	-	0.2	59.5	25.5	0.1

Table A2. Exalite and HDDMA-based scintillator formulations used for the second round of exploratory formulation studies to refine the plastic-forming and light-yielding fractions.

Scintillator	Component Fraction in Scintillator [wt%]						
	EJ-309	PPO	Exalite	IBOA	HDDMA	BPADMA	TPO
AFIT009	30	10	0.2	42	18	-	0.1
AFIT013	30	10	0.2	36	24	-	0.1
AFIT014	30	10	0.2	30	30	-	0.1
AFIT016	20	10	0.2	49	21	-	0.1
AFIT017	10	10	0.2	56	24	-	0.1
AFIT022	20	10	0.4	49	21	-	0.1
AFIT023	20	10	0.2	49	11	10	0.1
AFIT025	10	20	0.4	49	21	-	0.1
AFIT026	5	25	0.4	49	21	-	0.1

Table A3. Scintillator formulations used for the 2-level factorial study to optimize overall performance.

Scintillator	Component Fraction in Scintillator [wt%]						
	DIN	PPO	Exalite	IBOA	HDDMA	BPADMA	TPO
AFIT101	-	30	0.2	49	21	-	0.1
AFIT102	10	20	0.2	49	21	-	0.1
AFIT103	20	10	0.2	49	21	-	0.1
AFIT104	30	-	0.2	49	21	-	0.1
AFIT105	-	30	0.2	49	14	7	0.1
AFIT106	10	20	0.2	49	14	7	0.1
AFIT107	20	10	0.2	49	14	7	0.1
AFIT109	-	30	0.2	49	7	14	0.1
AFIT110	10	20	0.2	49	7	14	0.1
AFIT111	20	10	0.2	49	7	14	0.1
AFIT113	-	30	0.2	49	-	21	0.1
AFIT114	10	20	0.2	49	-	21	0.1
AFIT130	15	15	0.2	49	10.5	10.5	0.1
AFIT230	-	30	0.2	49	21	-	0.1
AFIT225	5	25	0.2	49	21	-	0.1
AFIT220	10	20	0.2	49	21	-	0.1
AFIT221	10	20	0.2	49	14	7	0.1

Table A4. Scintillator formulations used for the ethanol treatment study.

Scintillator	Component Fraction in Scintillator [wt%]						
	DIN	PPO	Exalite	IBOA	HDDMA	BPADMA	TPO
AFIT230	0	30	0.2	49	21	0	0.1
AFIT225	5	25	0.2	49	21	0	0.1
AFIT220	10	20	0.2	49	21	0	0.1
AFIT221	10	20	0.2	49	14	7	0.1

References

- Hamel, M.; Chapter Introduction—Overview on Plastic and Inorganic Scintillators. In *Plastic Scintillators*; Springer Nature: Cham, Switzerland, 2021; pp. 3–33.
- Hausladen, P.; Blackston, M. Passive and active fast-neutron imaging in support of APCI safeguards campaign. In *Oak Ridge National Laboratory*; Report No. ORNL/TM-2009/210; Oak Ridge National Laboratory: Oak Ridge, TN, USA, 2009.
- Beddar, S.; Tendler, I.; Therriault-Proulx, F.; Archambault, L.; Beaulieu, L., Recent Advances and Clinical Applications of Plastic Scintillators in the Field of Radiation Therapy. In *Plastic Scintillators: Chemistry and Applications*; Hamel, M., Ed.; Springer International Publishing: Cham, Switzerland, 2021; pp. 425–460. [\[CrossRef\]](#)
- Gibson, I.; Rosen, D.B.S. *Additive Manufacturing Technologies: 3D Printing, Rapid Prototyping, and Direct Digital Manufacturing*; Springer: Berlin/Heidelberg, Germany, 2015. [\[CrossRef\]](#)
- Ligon, S.C.; Liska, R.; Stampfl, J.; Gurr, M.; Mülhaupt, R. Polymers for 3D Printing and Customized Additive Manufacturing. *Chem. Rev.* **2017**, *117*, 10212–10290. [\[CrossRef\]](#) [\[PubMed\]](#)
- Mishnayot, Y.; Layani, M.; Cooperstein, I.; Magdassi, S.; Ron, G. Three-dimensional printing of scintillating materials. *Rev. Sci. Instrum.* **2014**, *85*, 085102. [\[CrossRef\]](#) [\[PubMed\]](#)
- Zhu, J.; Ding, Y.; Zhu, J.; Qi, D.; Su, M.; Xu, Y.; Bi, Y.; Lin, R.; Zhang, L. Preparation and characterization of a novel UV-curable plastic scintillator. *Nucl. Instrum. Methods Phys. Res. Sect. A* **2016**, *817*, 30–34. [\[CrossRef\]](#)
- Lee, S.; Son, J.; Kim, D.G.; Choi, J.; Kim, Y.K. Characterization of plastic scintillator fabricated by UV LED curing machine. *Nucl. Instrum. Methods Phys. Res. Sect. A* **2019**, *929*, 23–28. [\[CrossRef\]](#)
- Kim, D.G.; Lee, S.; Kim, Y.H.; Seon, S.J.; Sejin, J.; Jeong, J.Y.; Kim, Y.K. Scintillation Light Output of 3D Printed Plastic Scintillators. In Proceedings of the Transactions of the Korean Nuclear Society Spring Meeting, Jeju, Korea, 17–18 May 2018.

10. Kim, D.G.; Lee, S.; Park, J.; Son, J.; Kim, T.H.; Kim, Y.H.; Pak, K.; Kim, Y.K. Performance of 3D printed plastic scintillators for gamma-ray detection. *Nucl. Eng. Technol.* **2020**, *52*, 2910–2917. [[CrossRef](#)]
11. Kim, K.; Kim, D.G.; Lee, S.; Park, J.; Son, J.; Kim, Y.K. Neutron-Gamma Pulse Shape Discrimination Using 3D-Printed Plastic Scintillator with High-Concentration PPO. In Proceedings of the 2020 IEEE Nuclear Science Symposium and Medical Imaging Conference (NSS/MIC), Boston, MA, USA, 31 October–7 November 2020; pp. 1–3. [[CrossRef](#)]
12. Lim, A.; Mahl, A.; Latta, J.; Yemam, H.A.; Greife, U.; Sellinger, A. Plastic scintillators with efficient light output and pulse shape discrimination produced via photoinitiated polymerization. *J. Appl. Polym. Sci.* **2019**, *136*, 47381. [[CrossRef](#)]
13. Eljen Technology. Pulse Shape Discrimination EJ-276 & EJ-276G. Available online: <https://eljentechnology.com/products/plastic-scintillators/ej-276> (accessed on 4 November 2021).
14. Zaitseva, N.; Rupert, B.L.; Pawełczak, I.; Glenn, A.; Martinez, H.P.; Carman, L.; Faust, M.; Cherepy, N.; Payne, S. Plastic scintillators with efficient neutron/gamma pulse shape discrimination. *Nucl. Instrum. Methods Phys. Res. Sect. A* **2012**, *668*, 88–93. [[CrossRef](#)]
15. Zaitseva, N.; Glenn, A.; Mabe, A.; Carman, M.; Hurlbut, C.; Inman, J.; Payne, S. Recent developments in plastic scintillators with pulse shape discrimination. *Nucl. Instrum. Methods Phys. Res. Sect. A* **2018**, *889*, 97–104. [[CrossRef](#)]
16. Febbraro, M. 3D Printing of Photocurable Scintillating and Low-Background Materials. Presented at the CPAD Instrumentation Frontier Workshop, Stony Brook, NY, USA, 18–22 March 2021.
17. Frandsen, B.G. Capability Development for Advanced (n,x) Nuclear Data Measurements. Ph.D Thesis, Air Force Institute of Technology, Fort Belvoir, VA, USA, 2022.
18. van Loef, E.V.; Markosyan, G.; Shirwadkar, U.; Shah, K.S. Plastic Scintillators With Neutron/Gamma Pulse Shape Discrimination. *IEEE Trans. Nucl. Sci.* **2014**, *61*, 467–471. [[CrossRef](#)]
19. Laplace, T.; Goldblum, B.; Bevins, J.; Bleuel, D.; Bourret, E.; Brown, J.; Callaghan, E.; Carlson, J.; Feng, P.; Gabella, G.; et al. Comparative scintillation performance of EJ-309, EJ-276, and a novel organic glass. *J. Instrum.* **2020**, *15*, P11020. [[CrossRef](#)]
20. McCormack, O.; Giacomelli, L.; Croci, G.; Muraro, A.; Gorini, G.; Grosso, G.; Pasqualotto, R.; Cippo, E.P.; Rebai, M.; Rigamonti, D.; et al. Characterization and operational stability of EJ276 plastic scintillator-based detector for neutron spectroscopy. *J. Instrum.* **2021**, *16*, P10002. [[CrossRef](#)]
21. Chikkur, G.; Umakantha, N. A new method of determining the compton edge in liquid scintillators. *Nucl. Instrum. Methods* **1973**, *107*, 201–202. [[CrossRef](#)]
22. Dietze, G.; Klein, H. Gamma-calibration of NE 213 scintillation counters. *Nucl. Instrum. Methods Phys. Res.* **1982**, *193*, 549–556. [[CrossRef](#)]
23. Brown, J.A.; Goldblum, B.L.; Laplace, T.A.; Harrig, K.P.; Bernstein, L.A.; Bleuel, D.L.; Younes, W.; Reyna, D.; Brubaker, E.; Marleau, P. Proton light yield in organic scintillators using a double time-of-flight technique. *J. Appl. Phys.* **2018**, *124*, 045101. [[CrossRef](#)]
24. Pawełczak, I.; Ouedraogo, S.; Glenn, A.; Wurtz, R.; Nakae, L. Studies of neutron- γ pulse shape discrimination in EJ-309 liquid scintillator using charge integration method. *Nucl. Instrum. Methods Phys. Res. Sect. A* **2013**, *711*, 21–26. [[CrossRef](#)]
25. Winyard, R.; Lutkin, J.; McBeth, G. Pulse shape discrimination in inorganic and organic scintillators. I. *Nucl. Instrum. Methods* **1971**, *95*, 141–153. [[CrossRef](#)]
26. Sasano, M.; Nishioka, H.; Okuyama, S.; Nakazawa, K.; Makishima, K.; Yamada, S.; Yuasa, T.; Okumura, A.; Kataoka, J.; Fukazawa, Y.; et al. Geometry dependence of the light collection efficiency of BGO crystal scintillators read out by avalanche photo diodes. *Nucl. Instrum. Methods Phys. Res. Sect. A* **2013**, *715*, 105–111. [[CrossRef](#)]

Disclaimer/Publisher’s Note: The statements, opinions and data contained in all publications are solely those of the individual author(s) and contributor(s) and not of MDPI and/or the editor(s). MDPI and/or the editor(s) disclaim responsibility for any injury to people or property resulting from any ideas, methods, instructions or products referred to in the content.